11

Resonance Scattering Lidar

Makoto Abo

Graduate School of Engineering, Tokyo Metropolitan University,
1-1 Minami-Ohsawa, Hachioji-shi, Tokyo 192-0397, Japan
(abo@eei.metro-u.ac.jp)

11.1 Introduction

Resonance fluorescence is the process in which the energy of an incoming photon coincides with the energy of a transition in the level scheme of an atom, ion, or molecule, and is reemitted at the same or at some longer wavelength. In lidar, we consider only those cases in which both wavelengths are the same. Resonance fluorescence is widely used for analytical purposes because of the high, narrow peaks of the resonance lines. These result in high sensitivity and high selectivity of the analytical procedure. The resonance process implies both absorption, or a loss, and reemission, or scattering of the primary radiation. Resonance *absorption* is used in differential-absorption lidar, e.g., for the measurement of mercury [1] (see Chapter 7). Resonance *scattering* has had very few applications in lidar at low and middle altitudes, for a number of reasons. First, the resonance fluorescence process is most intense on atoms and ions which have few, but very intense, lines and not so well on molecules with vibrational and rotational degrees of freedom in which the oscillator strength is distributed over broad bands with a very high number of individual, but much less intense lines. Second, fluorescence lifetimes are relatively long, limiting the temporal resolution and thus range resolution of the lidar at low altitudes where high resolution is often required. Third, nonradiative (collision) deexcitation or quenching, with the resulting loss in intensity, is important at atmospheric pressure. Finally, free metal atoms or ions for which resonance fluorescence is most intense are not abundant in the lower layers of the atmosphere.

Conditions are different, however, in the high atmosphere. In 1969 Bowman et al. [2] made the first resonance-scattering lidar observation of an atomic layer of metallic sodium (Na) in the mesopause region at altitudes between 80 and 110 km using resonance-scattering lidar. In fact, the existence of a layer of sodium atoms in the mesopause region had already been deduced from observations at twilight by Chamberlain et al. in 1958 [3]. These findings were later confirmed by a number of researchers such as Sandford and Gibson in 1970 [4], Hake et al. in 1972 [5], Mégie and Blamont in 1977 [6], later by Beatty et al. [7] and Tilgner and von Zahn [8] in 1988, and by others. In the Southern hemisphere Clemesha et al. [9] made long-term observations of the Na layer for over 15 years. In the United States, high-resolution measurements by the group led by Gardner at the University of Illinois allowed the observation of wave-like structures that were interpreted as gravity waves [10]. They also observed the horizontal structure of the Na layer in equatorial and polar areas with an airborne Na lidar [11, 12]. At about the same time, an American and a French group became successful in observing metallic species other than Na such as potassium, lithium, calcium in atomic and ionic form, and iron (K, Li, Ca, Ca^+, Fe) [13–17]. Later, these and other groups carried out simultaneous determinations of the different atoms and ions and compared the results with data from high-atmosphere observations made with different instruments [18, 19]. Later, more atmospheric quantities than just atomic densities were extracted from the data. Lidar systems for the determination of temperature from the Doppler broadening of the Na D_2 lines were presented by Gibson et al. in 1979 [20], Fricke and von Zahn in 1985 [21], von Zahn and Neuber in 1987 [22], and She et al. in 1990 [23]. Later, the Na D_2 Doppler shift was also used to develop a highly accurate method for determining radial wind [24]. This considerably widened the field of applications of resonance scattering lidar in the high atmosphere.

11.2 The Mesospheric Na Layer: Methodology and Observations

For resonance scattering lidar, wavelength tunability is clearly required for the transmitting laser. In the early days, flashlamp-pumped dye lasers were used because they provided high pulse power and were tunable over a wide range of wavelengths. They could cover, in fact, the whole visible spectrum. Dyes from the rhodamine family showed large output power

and good stability characteristics, especially at wavelengths between 550 and 600 nm, which was ideal for the Na atom with its strong D_2 resonance line at 589 nm. Dye lasers directly pumped by flashlamps were used in the initial stage, but this type of laser was poorly suited for long, continuous observations because of the short lifetimes of the flashlamps and of the dyes, these latter being deteriorated by the intense light of the flashlamps of which only a small spectral band was converted to useful radiation. Thus, the light from the flashlamps was later replaced by the second harmonic of the output of a Nd:YAG laser. With this monochromatic radiation of a wavelength of 532 nm, higher excitation efficiency and longer dye life were achieved which allowed better observations. Figure 11.1 shows schematically the layout of a typical lidar for Na layer observations.

What makes a resonance scattering lidar differ significantly from other lidar systems is not only that it must allow precise tuning to the resonance line of the target atom or ion, it must also maintain a narrow linewidth for the whole duration of the observation. Table 11.1 lists the technical data of the Na layer observation lidar used at Tokyo Metropolitan University. The desired laser linewidth of approximately 2.5 pm is slightly less than the width of the Na D_2 line. If the laser linewidth becomes wider, the resonance-scattering efficiency quickly decreases, with a corresponding reduction of the lidar signal-to-noise ratio.

At an altitude around 90 km, scattering from aerosols and even atmospheric molecules can be ignored with respect to resonance

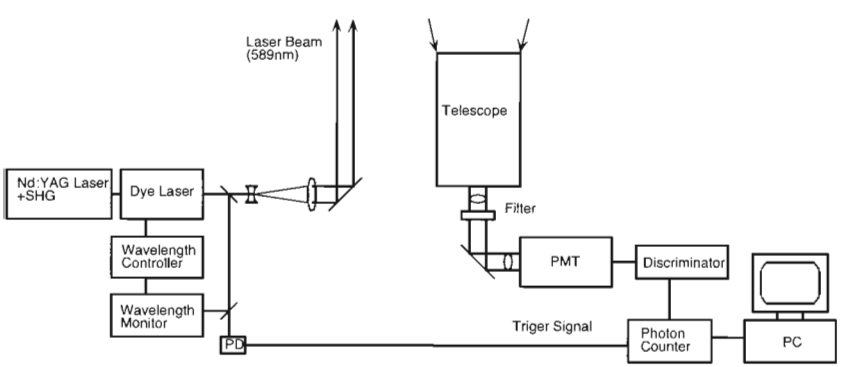

Fig. 11.1. Schematics of a typical resonance scattering lidar for mesospheric sodium measurements. PC data acquisition computer, PD photodiode, PMT photomultiplier tube.

Table 11.1. Technical data of the MTU resonance-scattering sodium lidar

Transmitter:	Laser	Nd:YAG SHG pumped dye
	Wavelength	589 nm
	Pulse energy	100 mJ/pulse
	Pulse repetition rate	10 Hz
	Linewidth	2.5 pm FWHM
	Pulse length	6 ns
	Beam divergence	0.2 mrad
Receiver:	Telescope	60 cm diameter Cassegrain
	Field of view	0.7 mrad
	Optical bandwidth	3.5 nm FWHM
Data Acquisition:	Type	Photon counting
	Range resolution	100 m

scattering. The lidar signal power from resonance backscattering at height z in this region can be described as

$$P(z) = \frac{P_0 A \eta T(z)^2 \rho_{\mathrm{Na}}(z) \sigma_{\mathrm{eff}}}{z^2}, \tag{11.1}$$

where $P(z)$ is the lidar receiver intensity, $P_0 = Ec/2$ the transmitting laser output if E is the pulse energy and c is the speed of light, A is the area of the receiving mirror, η the efficiency of the receiver system, $T(z)$ the transmission factor from the ground to height z, and $\rho_{\mathrm{Na}}(z)$ the number density of Na atoms at height z. This is the familiar lidar equation. For resonance-scattering lidar, however, the cross section must be replaced with the quantity

$$\sigma_{\mathrm{eff}} = \int g(\nu)\sigma(\nu, z)\mathrm{d}\nu = \int g'(\lambda)\sigma'(\lambda, z)\mathrm{d}\lambda, \tag{11.2}$$

which we call effective cross section. $g(\nu)$ or $g(\lambda)$ is the normalized spectral distribution of the laser power over the fluorescence line of the atom, and $\sigma(\nu, z)$ or $\sigma(\lambda, z)$ is the cross section distribution in the line which in principle shows a weak dependence on height z. Whether the wavenumber (ν) or wavelength notation (λ) is used is a matter of taste. The primes indicate that the functions are not the same, but the integral is the same. Figure 11.2 shows the relationship between the laser linewidth and the effective cross section.

Figure 11.3 is a plot of the raw lidar data of a height profile with echo from a layer of Na atoms with maximum centered around 90 km height. Signal contributions from aerosols can be totally ignored. For

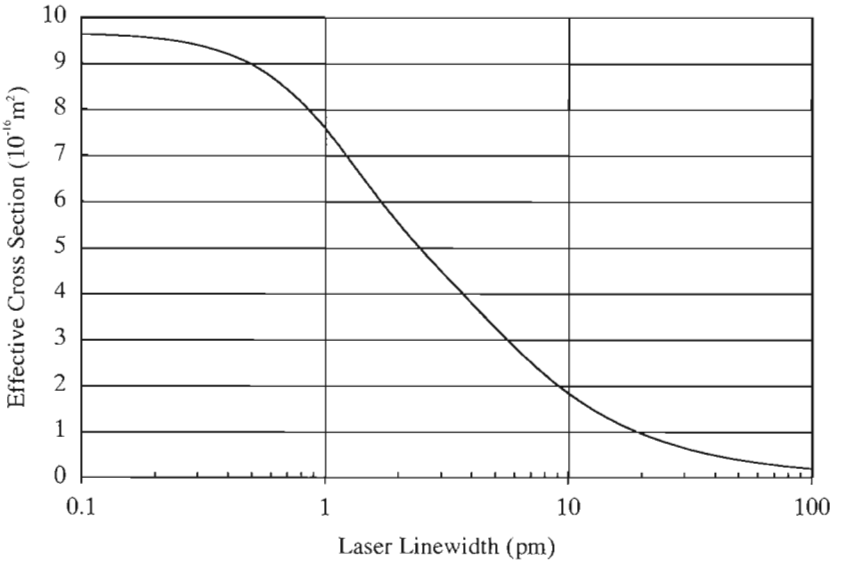

Fig. 11.2. Effective resonance cross section versus laser linewidth.

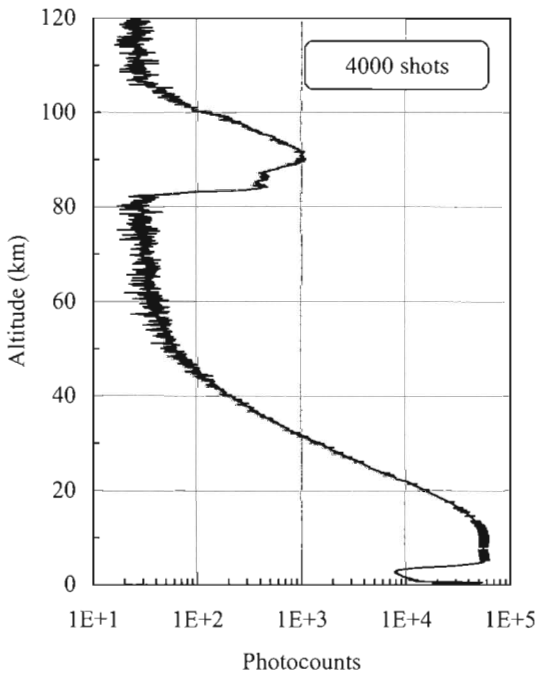

Fig. 11.3. Raw data of a sodium lidar profile (4000 shots).

the calculation of Na atomic density from the raw data, the signal at an altitude z_R is used at which molecular scattering is fully present and constitutes the only contribution to the lidar signal. This is normally an altitude around 30 to 35 km. This signal is given by

$$P(z_R) = \frac{P_0 A \eta T^2 \rho_M(z_R) \sigma_M}{z_R^2}. \tag{11.3}$$

$\rho_M(z_R)$ is the number density of atmospheric molecules at altitude z_R and σ_M is their Rayleigh scattering cross section. With the known density $\rho_M(z_R)$ the number density of the Na atoms is then easily determined by taking the ratio of Eqs. (11.1) and (11.3). The result is

$$\rho_{Na}(z) = \frac{P(z)\rho_M(z_R)\sigma_M z^2}{P(z_R)\sigma_{eff} z_R^2}. \tag{11.4}$$

In doing so, we had to use the assumption that the additional absorption by the sodium atoms in the transmission term can be neglected. This assumption is justified.

Figure 11.4 shows as an example the distribution of Na atom densities taken at Tokyo Metropolitan University on the night of 14 to 15 January 2004. It displays one Na atomic density profile every 8 minutes, from sunset to sunrise.

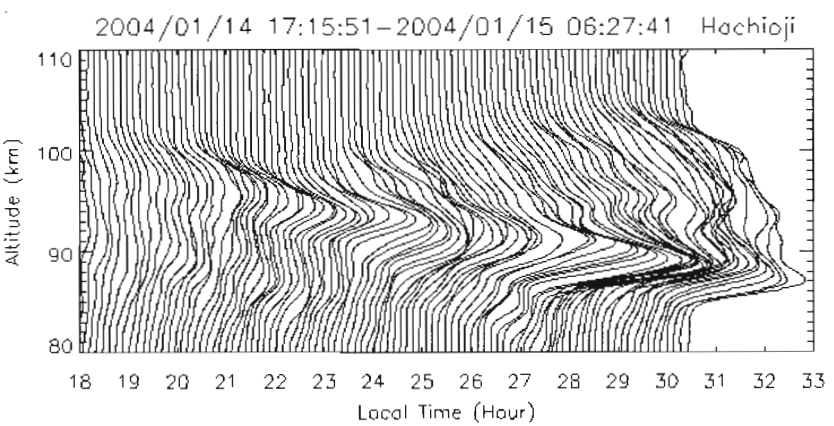

Fig. 11.4. Time series of mesospheric sodium layers observed at Tokyo in the night of 14 to 15 January 2004. Concentrations are in arbitrary units.

Daytime observations also are of considerable interest. Because of the intense skylight background and resulting low signal-to-noise ratio, such daytime measurements are not easy to make. Gibson and Sandford [25] used a Fabry–Perot etalon as a narrowband filter and were the first to present Na density profiles during daytime. In 1982 Clemesha et al. [26] and Granier and Mégie [27] and in 1987 Kwon et al. [28] continued such observations. However, there are not many cases of continuous observations reported because of the difficulties with etalon control and stabilization. In 1996, Chen et al. [29] successfully carried out daytime observations of the Na atomic layer in the mesopause region with relatively simple equipment, viz., a Faraday band-pass filter.

The filter consists of a Na atomic vapor cell in a magnetic field between crossed polarizers. The magnetic field Zeeman splits the energy levels, resulting in separate absorption lines for left and right circularly polarized light. We can consider the filter transmission in terms of circularly polarized light outside, between, and at the absorption lines. Outside these lines, the filter can be regarded as a Faraday rotator that uses Na vapor as the magneto-optic material inserted between crossed polarizers. The Na vapor exhibits rotary power only in the immediate vicinity of an absorption line, providing the 90-degree turn needed to pass the second polarizer. A simple peaked transmission spectrum is obtained when the filter parameters such as cell temperature and magnetic field are adjusted to provide a maximum rotation of 90 degrees. Away from the absorption line, the filter provides an out-of-band rejection determined by the extinction ratio of the crossed polarizers. In this way it becomes possible to take high-quality lidar data continuously day and night.

Among the geophysical questions directly related with Na atom abundance, the origin, distribution and wave-like behavior have dominated the discussions until now. As to the origin, diurnal and seasonal variations as well as the latitudinal distribution [30] give much insight into the effects responsible for the Na atom concentrations, but there is as yet no closed model of Na atom generation and transport, and the discussion of the related processes is far from being closed.

Gravity waves for which Na layers from the beginning of these investigations have been used as a near-ideal tracer, reveal the complex dynamics of the upper atmosphere, and both measurements and models continue to be an important subject in high-atmosphere research [31].

One of the most interesting and least understood phenomena in the mesopause region is perhaps the occurrence of sporadic Na layers (Na_s layers). Na_s layers are characterized by large density enhancements

in narrow altitude ranges, less than a few kilometers thick. Na_s layers were first observed at low and high, but not at mid-latitudes [32–36]. However, in 1995 observations by Nagasawa and Abo [37] indicated that the occurrence rate of Na_s layers at Hachioji, Tokyo (35.6 °N, 139.4 °E) (Fig. 11.5) can be comparable with those at low and high latitudes [32, 33, 38]. The formation mechanism of Na_s layers is actually under intense discussion. The high correlation observed between the occurrence of Na_s and sporadic E layers (E_s), which are the thin layers of enhanced ionization in the ionospheric E region, led to the hypothesis that the neutralization of a Na^+ (sodium ion) reservoir in the E_s layers was a source of large quantities of neutral Na atoms [36, 39, 40]. However, a recent observation at Arecibo Observatory showed that the appearance of an electron layer followed that of the correlated Na_s layer at its peak-abundance altitude [41]. Von Zahn et al. [42] also suggested that the Na_s layers at high latitude could originate from the release of Na by dust and smoke particles under the effect of energetic-particle bombardment. Even if this is correct, it remains difficult to explain the formation of Na_s layers at low latitudes by this mechanism [38]. Dynamical effects

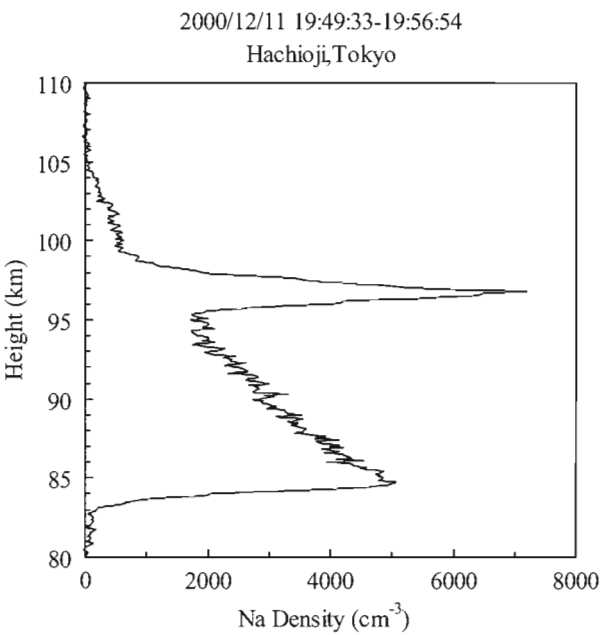

Fig. 11.5. Sporadic sodium layer observed at Tokyo on 11 December 2000.

associated with tides, gravity waves, and turbulence may contribute to the formation of Na_s layers [43, 44]. The significant difference in the occurrence rates at high and low from those at mid-latitudes has raised new questions as to the formation mechanisms of Na_s layers. Nagasawa and Abo suggested in 1995 that the occurrence of Na_s layers depends on geomagnetic rather than geographic latitude [37].

11.3 Observations of Other Metallic Layers

In addition to sodium, various other metal atoms and ions have also been considered as targets of mesosphere lidar observations. The most important ones are listed in Table 11.2. The Haute-Provence observation station in France (44°N) succeeded in observing metallic species such as K, Li, Ca, Ca ion, and Fe one after another, after Felix et al. in 1973 [13] and Mégie et al. in 1978 [14] had first seen and measured atomic potassium in the mesopause region using a ruby-laser-pumped dye laser. Suitable resonance lines are the ones at 769.9 and 766.5 nm. In practice it turns out that the weaker line (at 769.9 nm) is the better choice because the 766.5-nm line overlaps with an absorption line of the oxygen molecule. By tuning a flashlamp-pumped dye laser with 800 mJ output pulse energy to the Li resonance line of 670.8 nm, Jegou et al. [15] succeeded in observing Li at one thousandth the density of Na and in measuring the $^6Li/^7Li$ isotope ratio. They measured the isotopic ratio in meteor showers in order to obtain the cosmological isotopic ratio and compared it with the isotope ratio of terrestrial lithium. Granier et al. [16] could measure the atomic density of calcium with a dye laser at a wavelength of 422.7 nm

Table 11.2. Resonance lines of mesospheric metallic species used in resonance scattering lidar [45]

Metallic species	Resonance wavelength in air (nm)	Backscatter cross section ($m^2\ sr^{-1}$)
Fe	371.993	8.15×10^{-18}
Ca^+	393.366	1.12×10^{-16}
Ca	422.673	4.17×10^{-16}
Li	670.776	1.12×10^{-16}
Na	588.995	7.78×10^{-17}
K	769.897	7.51×10^{-17}

pumped by the third harmonic of a Nd:YAG laser. The same authors measured Ca ions with radiation of 393.4 nm wavelength [17]; to this end they mixed dye laser radiation of 624 nm with the 1064-nm Nd:YAG-laser fundamental. They finally succeeded in the measurement of Fe atomic density by mixing dye laser radiation of 572 nm and the Nd:YAG-laser fundamental of 1064 nm to produce 372.0 nm. Bills and Gardner [46] similarly measured Fe density in Illinois (40°N) using excimer-laser pumped dye lasers capable of high average output; their results were 5 to 8 times the Fe atomic densities observed by Granier et al. [17].

Gardner et al. [18] simultaneously measured Na, Fe, and Ca^+ densities and temperature (described in the following section), and Qian and Gardner [47] did a simultaneous observation of Ca and Na densities and temperature. Examples of their measurements are shown in Fig. 11.6. Alpers et al. [19] have been successful in simultaneously measuring the density of Ca and Ca^+. There are more examples of recent simultaneous observation with metallic atoms. Few of these use dye lasers any more. Instead, tunable solid-state lasers such as alexandrite and Ti:Al_2O_3 (or TiSa, for titanium-sapphire) lasers which are easier to use, particularly on mobile platforms, have taken over; e.g., Eska et al. [48] demonstrated the feasibility of measurements of latitudinal variations of K density with an alexandrite-laser-based lidar installed on board a vessel.

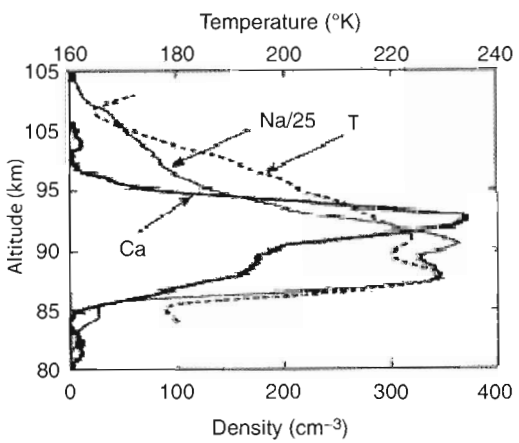

Fig. 11.6. Simultaneous common volume measurements of Ca density, Na density, and temperature (T) profiles. From Qian and Gardner, 1995 [47].

11.4 Measurements of Temperature and Wind with Resonance-Scattering Lidar

As shown in Fig. 11.7, the Na D_2 line undergoes Doppler broadening with atmospheric temperature; by measuring this broadening the temperature of the sodium layer can be determined. As the average number of collisions with atmospheric molecules at 90 km altitude is 10^4/s, it can be assumed that the Na is in local thermal equilibrium with its surroundings or, in other words, that its temperature is the same as that of the sodium.

The first to succeed in measuring the temperature of the sodium layer using resonance scattering lidar were Gibson et al. in 1979 [20]. Using a narrowband laser (laser linewidth approximately 100 MHz) they took resonance-scattering data at eight wavelengths within the Na D_2 line and fitted the measured data to the theoretical values of the Doppler-broadened line. However, their measurement range and height resolution were limited so they could only determine the average temperature in the central area of the sodium layer. Neuber et al. [49] later continuously measured the temperature in Andoya (69.3°N) using a similar method with excimer-laser-pumped dye lasers. Between the altitudes of

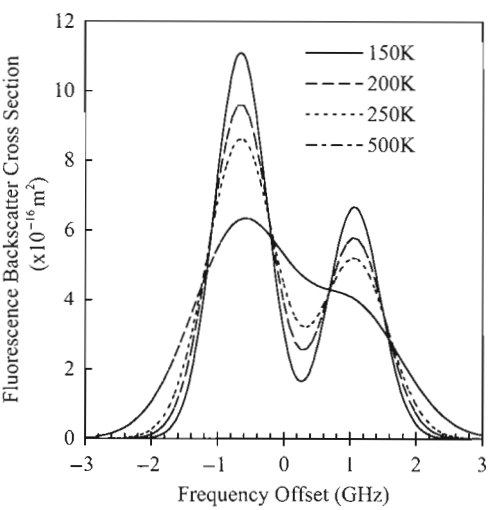

Fig. 11.7. Na D_2 Doppler-broadened fluorescence spectrum plotted as a function of frequency for four temperatures.

85 and 95 km and at a height resolution of 1 km, the accuracy of their temperature measurement was ±5 K.

She et al. [23] developed a method to measure temperature with higher accuracy. The principle of measurement has been described in detail by Bills et al. [50]. In order to obtain spectrally narrow laser emission, the authors injected radiation from a narrowband ring dye laser into a Nd:YAG-pumped pulsed dye laser. The frequency jitter obtained in this way was 1 MHz or less. Figure 11.8 is a diagram of their laser system. Their measurement device is also characterized by the utilization of Doppler-free saturated-absorption spectroscopy in a Na cell to alternately tune the lidar's optical transmission with high precision to the two most appropriate wavelengths within the Na D_2 line spectrum. Figure 11.9 shows the Na fluorescence spectrum from the Na vapor cell that is used. The spiked area in the spectrum is used as the tuning point. The final shape of the laser spectrum is then monitored with a Fabry–Perot etalon and corrected to maintain measurement accuracy. As a result, 5-minute measurements between 80 and 105 km and with 1 km range resolution yielded a temperature accuracy of ±1 K near the sodium peak of the Na layer and ±3 K elsewhere.

Using this technology in connection with the Faraday band-pass filter described in Section 2, daytime and nighttime measurements of the temperature were obtained. The results were quite different from those of conventional models. She et al. [24] further improved the Na temperature measuring device to measure the radial velocity with which the sodium layer moves, or wind. She et al. [51] provided eight-year climatology data of temperature profiles in the mesopause region. Temperature

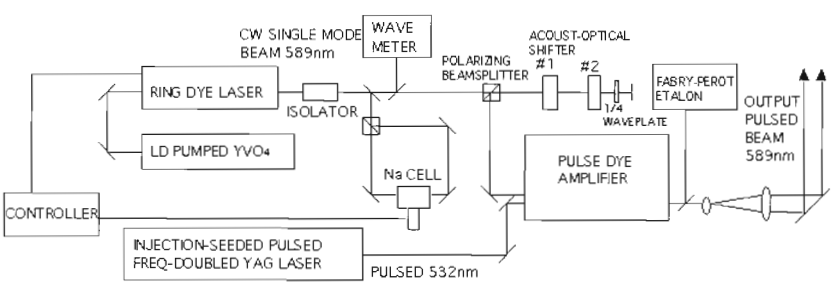

Fig. 11.8. Block diagram of the Na temperature lidar transmitter.

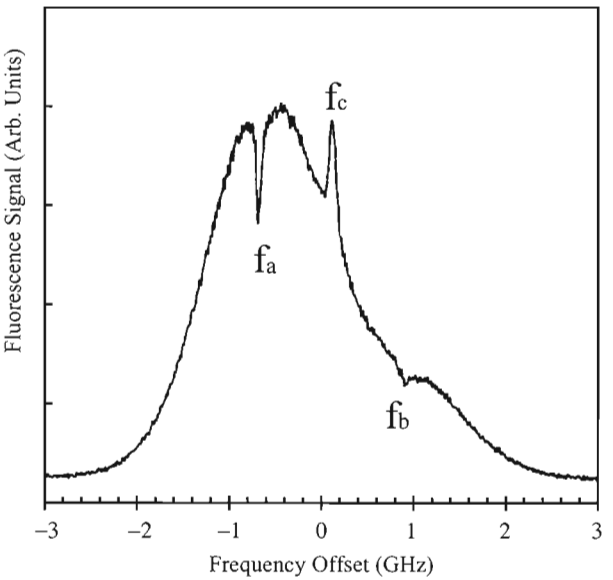

Fig. 11.9. The measured Na vapor cell fluorescence spectrum. The labels denote the Doppler-free feature at the D_2a peak (fa), crossover resonance (fc), and D_2b peak (fb).

contours support a two-level thermal structure. Examples of temperature measurements are shown in Fig. 11.10 [52].

Von Zahn and Höffner [53] used another element, potassium, to measure temperature. They employed a different measurement scheme with tunable solid-state lasers that are easier to maintain and operate than dye lasers.

Kawahara et al. [54] succeeded in temperature measurements over the Syowa station (69°S, 39°E) in Antarctica using a Na resonance line generated by sum-frequency mixing of two injection-seeded pulsed Nd:YAG lasers.

Gelbwachs [55] proposed to measure mesopause temperatures by determination of the Boltzmann factor instead of the Doppler broadening of a resonance line, preferably on iron. Gardner et al. [56] applied the method in an airborne lidar to the measurement of Leonid meteor trails and for observations over Antarctica [57]. The advantage of this method is that laser wavelength tuning need not be extremely accurate; however, there is the disadvantage that the resonance scattering cross sections of the two wavelengths used in the measurement (372 nm and 374 nm) are small and the echoes are weak.

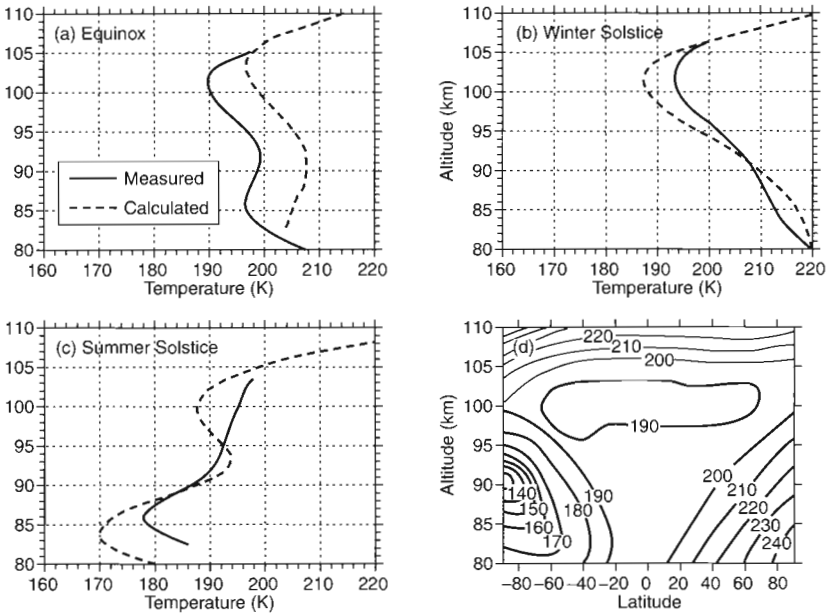

Fig. 11.10. Calculated and measured nighttime averaged temperature profiles over Fort Collins, CO (41°N, 105°W) for (a) equinox, (b) winter, (c) summer, along with calculated altitude-latitude plots of zonal mean temperature contours in the mesopause region for December solstice solar cycle minimum geomagnetic quiet conditions, in (d). From She et al. [52].

11.5 Summary and Future Prospects

In addition to the possibility of measuring the primary target of resonance-scattering lidar systems, i.e., the layers of metal atoms and ions in the mesopause region, now other parameters such as temperature and wind and their temporal and spatial distribution can also be determined. This greatly increased the range of investigations in the high atmosphere that can be tackled: dynamics, climatologies, meteoric material and its nature, quantity, frequency and time distribution of occurrence, and origin, to name just a few.

Of all competing technologies for measurements in this part of the atmosphere, resonance-fluorescence lidar combines such properties as good accuracy, specificity, resolution, independence from many perturbing conditions that affect other measurement schemes, safe operation from the ground, and low cost. It is thus ideally suited to supplement investigations made with other equipment that do not share these assets.

Examples are the middle and upper atmosphere (MU) radar [58], medium frequency (MF) radar [59], and CCD cameras [60]. This is certainly one reason why resonance-scattering lidars are being built and used in various parts of the world.

Resonance-scattering lidars, despite all their desirable features, suffer from two disadvantages. One is the fact that, because of ozone absorption, they cannot use excitation wavelengths much shorter than 300 nm; even high-power systems with large receiver telescopes will not extend that limit dramatically. The other disadvantage is that they do not work in cloudy weather. Both shortcomings are overcome when the systems are taken on high-flying planes or, better, satellites [61]. Work is in preparation or under way for the development of highly reliable, full solid-state Na lidar systems that meet the requirements for unattended operation [62, 63].

These technological improvements, however, are not the only direction in which resonance-fluorescence lidars develop. There are new physical challenges as well. An example is the work by Brinksma et al. [64] who were the first to succeed in the observation of OH molecules in the mesosphere using resonance-scattering lidars with excimer lasers. It might thus be possible to extend the range of target substances to other fluorescent molecules. Finally, as an example of application in areas outside the field of atmospheric science, laser guide stars are being developed in which a system similar to a resonance-scattering lidar targeting mesospheric Na layers is used. The resonance scattering from the Na layer can provide the beacon for adaptive-optics compensation of atmospheric distortion [65].

References

[1] H. Edner, G.W. Faris, A. Sunesson, et al.: Appl. Opt. **28**, 921 (1989)
[2] M.R. Bowman, A.J. Gibson, M.C.W. Sandford: Nature **221**, 456 (1969)
[3] J.W. Chamberlain, D.M. Hunten, J.E. Mack: J. Atmos. Terr. Phys. **12**, 153 (1958)
[4] M.C.W. Sandford, A.J. Gibson: J. Atmos. Terr. Phys. **32**, 1423 (1970)
[5] R.D. Hake, Jr., D.E. Arnold, D.W. Jackson, et al.: J. Geophys. Res. **77**, 6839 (1972)
[6] G. Mégie, J.E. Blamont: Planet. Space Sci. **25**, 1093 (1977)
[7] T.J. Beatty, R.E. Bills, K.H. Kwon, et al.: Geophys. Res. Lett. **15**, 1137 (1988)
[8] C. Tilgner, U. von Zahn: J. Geophys. Res. **93**, 8439 (1988)
[9] B.R. Clemesha, D.M. Simonich, P.P. Batista: Geophys. Res. Lett. **19**, 457 (1992)
[10] C.S. Gardner, D.G. Voelz: J. Geophys. Res. **92**, 4673 (1987)
[11] T.J. Kane, C.A. Hostetler, C.S. Gardner: Geophys. Res. Lett. **18**, 1365 (1991)
[12] Y.Y. Gu, J. Qian, G.C. Papen, et al.: Geophys. Res. Lett. **22**, 2805 (1995)

[13] F. Felix, F.W. Keenliside, G. Kent, et al.: Nature **246**, 345 (1973)
[14] G. Mégie, F. Bos, J.E. Blamont, et al.: Planet. Space Sci. **26**, 27 (1978)
[15] J.P. Jegou, M.L. Chanin, G. Mégie, et al.: Geophys. Res. Lett. **7**, 995 (1980)
[16] C. Granier, J.P. Jegou, G. Mégie: Geophys. Res. Lett. **12**, 655 (1985)
[17] C. Granier, J.P. Jegou, G. Mégie: Geophys. Res. Lett. **16**, 243 (1989)
[18] C.S. Gardner, T.J. Kane, D.C. Senft, et al.: J. Geophys. Res. **98**, 16865 (1993)
[19] M. Alpers, J. Höffner, U. von Zahn: Geophys. Res. Lett., **23**, 567 (1996)
[20] A.J. Gibson, L. Thomas, S. Bhattachacharyya: Nature **281**, 131 (1979)
[21] K.H. Fricke, U. von Zahn: J. of Atmos. Terr. Phys. **47**, 499 (1985)
[22] U. von Zahn, R. Neuber: Beitr. Phys. Atmosph. **60**, 294 (1987)
[23] C.Y. She, R.E. Bills, H. Latifi, et al.: Geophys. Res. Lett. **17**, 929 (1990)
[24] C.Y. She, J.R. Yu: Geophys. Res. Lett. **21**, 1771 (1994)
[25] A.J. Gibson, M.C.W. Sandford: Nature **239**, 509 (1972)
[26] B.R. Clemesha, D.M. Simonich, P.P. Batista, et al.: J. Geophys. Res. **87**, 181 (1982)
[27] C. Granier, G. Mégie: Planet. Space Sci. **30**, 169 (1982)
[28] K.H. Kwon, C.S. Gardner, D.C. Senft, et al.: J. Geophys. Res. **92**, 8781 (1987)
[29] H. Chen, M.A. White, D.A. Krueger, et al.: Opt. Lett. **21**, 1093 (1996)
[30] D.M. Simonich, B.R. Clemesha, V.W.J.H. Kirchhoff: J. Geophys. Res. **84** (A4), 1543 (1979)
[31] X. Hu, A.Z. Liu, C.S. Gardner, et al.: Geophys. Res. Lett. **29**, 2169 (2002)
[32] P.P. Batista, B.R. Clemesha, I.S. Batista, et al.: J. Geophys. Res. **94**, 15349 (1989)
[33] G. Hansen, U. von Zahn: J. Atmos. Terr. Phys. **52**, 585 (1990)
[34] T.J. Kane, C.S. Gardner, Q. Zhou, et al.: J. Atmos. Terr. Phys. **55**, 499 (1993)
[35] R.L. Collins, T.J. Hallinan, R.W. Smith, et al.: Geophys. Res. Lett. **23**, 3655 (1996)
[36] C.J. Heinselman, J.P. Thayer, B.J. Watkins: Geophys. Res. Lett. **25**, 3059 (1998)
[37] C. Nagasawa, M. Abo: Geophys. Res. Lett. **22**, 263 (1995)
[38] K.H. Kwon, D.C. Senft, C.S. Gardner: J. Geophys. Res. **93**, 14199 (1988)
[39] U. von Zahn, T.L. Hansen: J. Atmos. Terr. Phys. **50**, 93 (1988)
[40] R.M. Cox, J.M.C. Plane: J. Geophys. Res. **103**, 6349 (1998)
[41] J.S. Friedman, S.A. Gonzalez, C.A. Tepley, et al.: Geophys. Res. Lett. **27**, 449 (2000)
[42] U. von Zahn, P. von der Gathen, G. Hansen: Geophys. Res. Lett. **14**, 76 (1987)
[43] B.R. Clemesha, P.P. Batista, D.M. Simonich: Geophys. Res. Lett. **15**, 1267 (1988)
[44] Q. Zhou, J.D. Mathews: J. Atmos.Terr. Phys. **57**, 1309 (1995)
[45] U. von Zahn, J. Höffner, W.J. McNeil: Meteor trails as observed by lidar. In: *Meteors in the Earth's Atmosphere*, E. Murad, I.P. Williams, eds. (Cambridge University Press 2002), p. 149
[46] R.E. Bills, C.S. Gardner: Geophys. Res. Lett. **17**, 143 (1990)
[47] J. Qian, S. Gardner: J. Geophys. Res. **100** (D4), 7453 (1995)
[48] V. Eska, U. von Zahn, J.M.C. Plane: J. Geophys. Res. **104** (A8), 17,173 (1999)
[49] R. Neuber, P. von der Gathen, U. von Zahn: J. Geophys. Res. **93**, 11,093 (1988)
[50] R.E. Bills, C.S. Gardner, C.Y. She: Opt. Eng. **30**, 13 (1991)
[51] C.Y. She, S. Chen, Z. Hu, et al.: Geophys. Res. Lett. **27**, 3289 (2000)
[52] C.Y. She, J.R. Yu, D.A. Krueger, et al.: Geophys. Res. Lett. **22**, 377 (1995)
[53] U. von Zahn, J. Höffner: Geophys. Res. Lett. **23**, 141 (1996)
[54] T.D. Kawahara, T. Kitahara, F. Kobayashi, et al.: Geophys. Res. Lett. **29**, 1709 (2002)

[55] J.A. Gelbwachs: Appl. Opt. **33**, 7151 (1994)
[56] C.S. Gardner, G.C. Papen, X. Chu, et al.: Geophys. Res. Lett. **28**, 1199 (2001)
[57] X. Chu, W. Pan, G. Papen, et al.: Geophys. Res. Lett. **27**, 1807 (2000)
[58] S.P. Namboothiri, T. Tsuda, M. Tsutsumi, et al.: J. Geophys. Res. **101**, 4057 (1996)
[59] R.L. Collins, D. Thorsen, S.J. Franke: J. Geophys. Res. **102** (D14), 16,583 (1997)
[60] J.H. Hecht, R.L. Walterscheid, D.C. Fritts, et al.: J. Geophys. Res. **102** (D6), 6655 (1997)
[61] S.-D. Yeh, E.V. Browell: Appl. Opt. **21**, 2365 (1982)
[62] P.H. Chiu, A. Magana, J. Davis: Opt. Lett. **19**, 2116 (1994)
[63] R.W. Farley, P.D. Dao: Appl. Opt. **34**, 4269 (1995)
[64] E.J. Brinksma, Y.J. Meijer, I.S. McDermid, et al.: Geophys. Res. Lett. **25**, 51 (1998)
[65] C.S. Gardner: Proceedings of the IEEE **77**, 408 (1989)